ELSEVIER

Coordination Chemistry Reviews 233–234 (2002) 193–206

COORDINATION CHEMISTRY REVIEWS

www.elsevier.com/locate/ccr

Polynuclear coordination complexes—from dinuclear to nonanuclear and beyond

Laurence K. Thompson *

Department of Chemistry, Memorial University, St. John's, Nfld, Canada A1B 3X7

Received 19 September 2001; accepted 15 March 2002

Contents

Abstract

Polytopic ligands based on aromatic or open chain diazine and alkoxo-fragments form an ideal focus for the simultaneous coordination of metal centers in contiguous groupings, juxtaposed closely enough that magnetic spin–spin exchange occurs between adjacent pairs of metal ions. Examples of polynuclear complexes M_n ($n = 2$–9) will be discussed in terms of their structures, and principally their magnetic properties, with a focus on self-assembly reactions. Ligand design elements that lead to predictable cluster and grid structures will be emphasized. Magneto-structural studies and correlations will be highlighted with antiferromagnetic and ferromagnetic examples, in addition to recent studies with high nuclearity grids and clusters. Ferromagnetic grids with high spin ground states present exciting possibilities for applications of these nano-scale molecular systems in, e.g. information storage technology.

1. Introduction

Coordination chemists have been fascinated by the ability of organic molecules with donor function (ligands) to sequester metal ions, and impart unusual properties, e.g. color, redox behavior, catalytic properties, magnetic properties etc. to the products, and the link between inorganic coordination chemistry and biology was indelibly forged when it was discovered that natural ligands bound specific metal ions in natural life processes [1]. Single metal ions embraced by a simple monodentate or chelating ligand environment are commonplace, and in such systems individual metal centers are usually too far away for any spin coupling between paramagnetic metal ions to occur. Polynucleating ligands, on the other hand, have structural attributes that combine separate coordination pockets, and in cases where they are contiguously arranged, metal ions are bound in close proximity, and can be linked directly by endogenous or exogenous ligand fragments, leading

* Tel.: +1-709-735-8750; fax: +1-709-737-3702
E-mail address: lthomp@mun.ca (L.K. Thompson).

0010-8545/02/$ - see front matter
PII: S0010-8545(02)00101-7

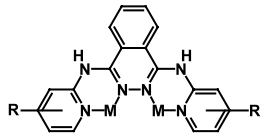

PAPR

R = H;3Me;4Me;5Me;6Me;4,6-DiMe

Scheme 1.

to spin communication between metals. Classic cases involving biological ligands include hemocyanin and ascorbate oxidase, where strong antiferromagnetic coupling occurs between adjacent copper(II) centers via single atom 'oxygen' bridges [1,2].

Our interest in polynuclear complexes started with a class of dinucleating phthalazine ligands (PAPR; Scheme 1), where the adjacent positioning of the diazine ring nitrogen atoms provides an ideal focus for the simultaneous coordination of two metal ions in close proximity. Spin coupled complexes are produced with Co(II), Ni(II) and Cu(II) salts, with examples of antiferromagnetic and ferromagnetic systems, depending on co-ligands and dinuclear center geometries [3–46]. Fused aromatic diazines (e.g. phthalazines, pyridazines [3–40]) effectively fix the coordination positions of the nitrogen donors and lead to limited flexibility of the dinuclear center dimensions. Open chain diazine ligands, however, (Scheme 2) allow considerable rotational flexibility of the metal magnetic orbitals leading to unique exchange situations, which depend on alignment of the diazine nitrogen 'p' orbitals [41–47].

Using the ligand as the focus for the nuclearity of the complex, this class of ligand can effectively be doubled by using a benzo-dipyridazine ligand core (Scheme 3), effectively also doubling the coordinating capacity of the dinucleating ligands, and allowing four metal centers to coordinate and couple magnetically [31]. Extending this approach to higher nuclearities is difficult on the basis of a single ligand, and other approaches including metal template techniques and self-assembly can achieve higher nuclearity complexes.

The purpose of this review is to summarize the approaches we have taken to produce polynuclear and 'high nuclearity' coordination complexes, with an emphasis on the creation of polynuclear systems with metal ion centers in close proximity, and an interpretation of magnetic properties as a function of structural features,

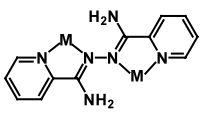

PAHAP

Scheme 2.

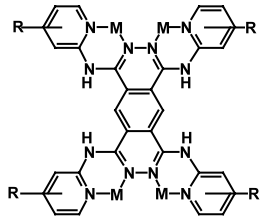

diPAPR

R = H;4Me;5Me;6Me

Scheme 3.

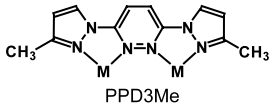

PPD3Me

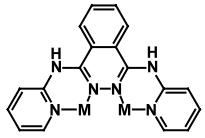

PAP

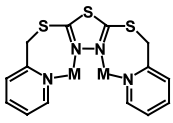

DMPTD

Scheme 4.

and in particular the correlations that exist between structural and magnetic properties.

2. Dinuclear complexes

Heterocyclic 1,2-diazine ligands based on pyridazine, phthalazine and thiadiazole (Schemes 1 and 4) bind two metals in close proximity, and generate an ideal model situation for the study of spin–spin exchange between adjacent metal centers as a function of the N_2 diazine bridge and exogenous bridging groups X (X = Cl, Br, OH, IO_3, SO_4, N_3). A rich coordination chemistry has emerged over the last 30 years [3–40], and with copper the complexes have provided a useful probe for magne-

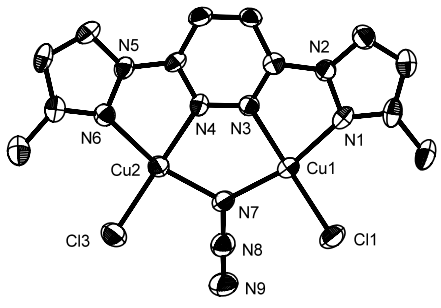

Fig. 1. Structural representation of $[Cu_2(PPD3Me)(\mu_2\text{-}1,1\text{-}N_3)Cl_2]Cl$ (**1**).

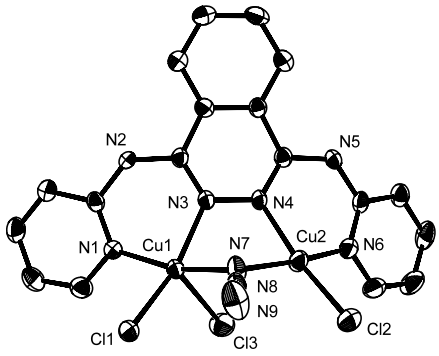

Fig. 2. Structural representation of $[Cu_2(PAP)(\mu_2\text{-}1,1\text{-}N_3)(\text{-}Cl)Cl_2]$ (**2**).

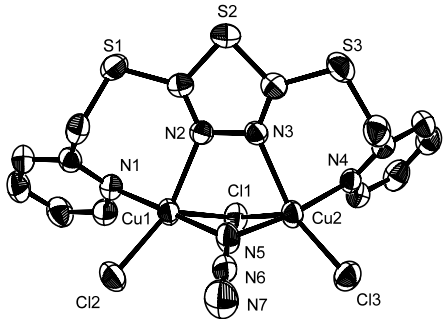

Fig. 3. Structural representation of $[Cu_2(DMPTD)(\mu_2\text{-}1,1\text{-}N_3)(\mu\text{-}Cl)Cl_2]$ (**3**).

tostructural correlations. Ligands like PPD3Me, PAP, and DMPTD (Scheme 4) create dinuclear centers with varying chelate rings sizes at each metal ion (5, 6 and 7, respectively), which leads to a situation where the metal ion separations get progressively shorter. This produces a varying Cu–X–Cu bridging angle (X = exogenous bridging group) in proportion to the Cu–Cu distances. Figs. 1–3 illustrate this situation for the three ligand types in the complexes $[Cu_2(PPD3Me)(\mu_2\text{-}1,1\text{-}N_3)Cl_2]Cl$ (**1**), $[Cu_2(PAP)(\mu_2\text{-}1,1\text{-}N_3)(\mu\text{-}Cl)Cl_2]$ (**2**), $[Cu_2(DMPTD)(\mu_2\text{-}1,1\text{-}N_3)(\mu\text{-}Cl)Cl_2]$ (**3**), with Cu–N_3–Cu angles of 124.1, 107.9 and 105.9°, respectively. $2J$ values are found to be −780, −40 and +170 cm^{-1}, respectively, within this group ($H_{ex} = -2J\{S_1S_2\}$). For a large series of equatorially dibridged (diazine/azide) complexes, where X = μ-1,1-N_3 a very wide variation in Cu–N_3–Cu angles was found (101.0–124.1°), with a corresponding change in exchange integral from $2J = +170$ to -1100 cm^{-1}. The crossover from ferromagnetic to antiferromagnetic exchange occurs at ∼108° associated with the azide bridge, and a reasonable linear relationship was found between the exchange integral and the bridge angle [35–40]. This result is in essential agreement with extended Hückel calculations, and the 'accidental orthogonality' principle resulting from early studies by Hatfield [47] on dihydroxy-bridged dicopper(II) complexes and Kahn [48] on di-μ_2-1,1-N_3 bridged dicopper(II) complexes, where calculated angles for 'accidental orthogonality' occurred at 92 and 103°, respectively. More recent studies suggested that 'spin polarization' effects were a dominant feature of the exchange process, leading to a situation where at all Cu–N_3–Cu angles ferromagnetic coupling should prevail [49,50]. However, polarized neutron studies [51], and DFT studies [52] on bis-(μ_2-1,1-N_3) bridged dicopper(II) systems indicate that while spin polarization may play a role, electron delocalization effects clearly exert a controlling influence in the exchange process, supporting the accidental orthogonality principle. A similar class of hydroxo-bridged complexes of ligands like PAP and PPD3Me show an equivalent trend, with Cu–O–Cu bridge angles in the range 100–125° and $-2J$ in the range 190–1300 cm^{-1}. Dominant antiferromagentic coupling in this range of angles is consistent with Hatfield's results, and the lower angle of accidental orthogonality for the $\mu_{1,2}$-OH bridge [27].

Ligands like PAHAP (Scheme 2) with N–N single bonds, as opposed to heterocyclic diazines, have a great deal of rotational flexibility, and in principal several different coordination modes. The dinuclear complex $[Cu_2(PAHAP)(NO_3)_2(H_2O)_6]$ $(NO_3)_2$ (**4**) (Fig. 4) has an 'open' structure in which two six-coordinate copper(II) centers are bridged by a single N–N bond, and steric and lattice hydrogen bonding interactions are the only forces controlling the relative rotation of the copper magnetic planes (100.2° twist between the (Cu1–N1–N2–O1–O2) magnetic planes). This compound exhibits antiferromagnetic exchange ($2J = -27.4$ cm^{-1}). The complex $[Cu_2(PAHAP)Br_4]\cdot H_2O$ (**5**) (Fig. 5) has a constrained 'closed' structure, resulting from a significant axial Cu–Br bridging interaction, producing a much smaller rotational angle τ between the metal magnetic planes (75.0°). In contrast this compound exhibits significant intramolecular ferromagnetic exchange ($2J = 22$ cm^{-1}) [41]. An expanded study invol-

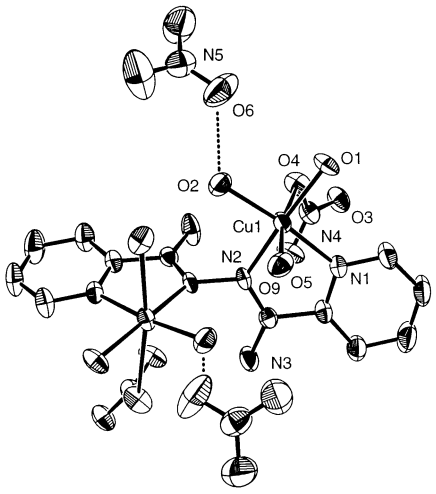

Fig. 4. Structural representation of $[Cu_2(PAHAP(NO_3)_2(H_2O)_6]$-$(NO_3)_2$ (**4**).

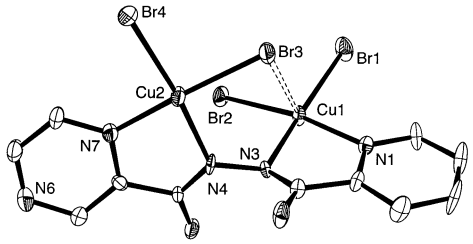

Fig. 5. Structural representation of $[Cu_2(PAHAP)Br_4] \cdot H_2O$ (**5**).

ving related ligands and various co-ligands produced a series of related derivatives with rotational angles (τ) in the range 70–170°, leading to a linear correlation between exchange integral and τ, supported by extended Hückel calculations [41,42]. This was related directly to the overlap situation between the copper magnetic (e.g. $d_{x^2-y^2}$) orbitals and the nitrogen p-orbitals in the diazine bridge, and the relative orientation of the nitrogen p-orbitals as a result of the collective steric and bonding effects. Further dinuclear complexes with Mn(II), Fe(II), Fe(III), Co(II) and Ni(II) salts of, e.g. PAHAP have a M_2L_3 spiral structure, with two six-coordinate metal ions bridged by three N–N single bonds. The complex $[Mn_2(PAHAP)_3](ClO_4)_4 \cdot 5H_2O$ (**6**) (Fig. 6) shows an acute twist of the metal magnetic orbitals around the N–N bonds (Mn–N–N–Mn torsional angles 46.3, 43.2°, consistent with the observed ferromagnetic interaction between the Mn(II) centers ($2J = 2.1$ cm^{-1}). An isostructural Ni(II) complex showed no intramolecular exchange [43].

3. Trinuclear complexes

Designing ligands that specifically form trinuclear complexes requires that there are three coordination compartments. Ligands like 2POAP (Scheme 5) can be synthesized quite readily from pyridine-2,6-dicarboxylic

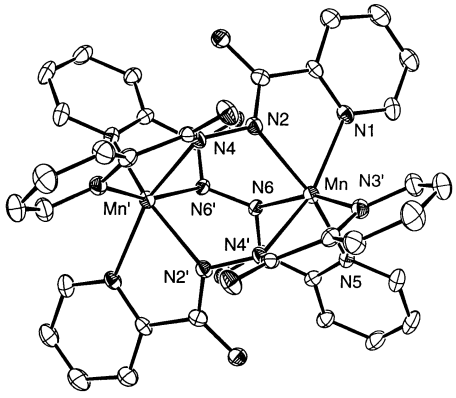

Fig. 6. Structural representation of $[Mn_2(PAHAP)_3](ClO_4)_4 \cdot 5H_2O$ (**6**).

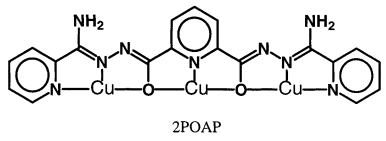

2POAP

Scheme 5.

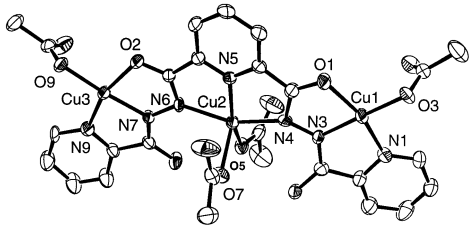

Fig. 7. Structural representation of $[Cu_3(2POAP\text{-}2H)\ (CH_3COO)_4] \cdot 3H_2O$ (**7**).

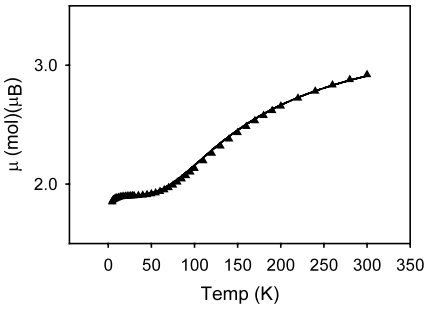

Fig. 8. Magnetic data for **7** (see text for fitted parameters).

acid hydrazide, and have a linear, contiguous arrangement of three coordination pockets [53]. Reaction of 2POAP with excess CuX_2 ($X = CH_3COO$, BF_4) produces green crystals of $[Cu_3(2POAP–2H)\ (CH_3COO)_4] \cdot 3H_2O$ (**7**) and $[Cu_3(2POAP–2H)(H_2O)(DMF)_3(CH_3OH)_2](BF_4)_4$ (**8**), respectively. The structure of **7** (Fig. 7) shows the two external copper(II) centers bridged by N–N single bonds to the central copper [54].

The variable temperature magnetic properties have been interpreted in terms of a linear exchange model (Eq. (1)), in which coupling between the external copper ions is assumed to be insignificant ($J' = 0$). The variation of magnetic moment (per mole) as a function of temperature for **7** is shown in Fig. 8. A good fit of the data gave $g = 2.19(1)$, $J = -75.5(2)$ cm^{-1}, $\theta = -0.2$ K, $\rho = 0.015$, $N\alpha = 180 \times 10^{-6}$ emu.mol^{-1}, $10^2R = 0.6(R = [\Sigma(\chi_{obs} - \chi_{calc.})^2/\Sigma\chi^2_{obs}]^{1/2})$ (the solid line in Figure 8 was calculated with these

$$H_{ex} = -2J[S_1 \cdot S_2 + S_2 \cdot S_3] - 2J'[S_1 \cdot S_3] \quad (1)$$

parameters; θ is a Weiss-like temperature correction defining weak intermolecular

$$\chi_m = \frac{Ng^2\beta^2}{3k(T-\theta)}\left[\frac{10e^{(x)} + e^{(-2x)} + 1}{2e^{(x)} + e^{(-2x)} + 1}\right](1-\rho) + \left(\frac{3Ng^2\beta^2}{4kT}\right)\rho + \mathrm{TIP}x = J/kT \quad (2)$$

exchange, ρ is the fraction of paramagnetic impurity, TIP is temperature independent paramagnetism). The strong antiferromagnetic exchange in this compound, and **8** ($J = -78.4\ \mathrm{cm}^{-1}$), is associated with the large C–N–N–Cu torsional angles (160–170°), and clearly consistent with the previous dinuclear N–N bridged copper(II) examples [41–46].

4. Tetranuclear complexes

4.1. Tetranucleating ligands

Ligands of the type diPAPR (Scheme 3) are clearly pre-organized to attract four metal ions, based on the preference of PAPR ligands to produce dinuclear complexes. Reaction of diPAP4Me with a large excess of $Cu(CF_3SO_3)_2$ in water gave a green solution, from which green crystals of $[Cu_4(diPAP4Me)(\mu\text{-}OH)_2(H_2O)_8](CF_3SO_3)_6$ (**9**) formed. The structure (Fig. 9) reveals four square-pyramidal copper(II) ions bound in a bis-dinuclear fashion, with the copper magnetic ($d_{x^2-y^2}$) orbitals directly connected to the bridging heterocyclic diazine and OH groups. Variable temperature magnetic data showed a broad maximum in the χ_m at ~250 K, indicating strong intramolecular antiferromagnetic exchange. The data were fitted to a rectangular model (Scheme 6) based on the exchange Hamiltonian Eq. (3), in which diagonal and lateral exchange

$$H_{ex} = -2J1(S_1 \cdot S_2 + S_3 \cdot S_4) - 2J2(S_1 \cdot S_4 + S_2 \cdot S_3) \quad (3)$$

terms are assumed to be the same. Strong antiferromagnetic exchange was observed ($J1 = -167(3)\ \mathrm{cm}^{-1}$, $J2 = -60(5)\ \mathrm{cm}^{-1}$), with $J1$ accounting for the expected exchange between each pair of copper(II) ions via the hydroxide bridge (Cu–OH–Cu 116.3°). In this and other related complexes a significant cross ligand, antiferromagnetic exchange term ($J2$) was required for a good data fit, indicating the importance of the fused aromatic ring system in propagating spin coupling over the eight bond connection between the dinuclear halves of the molecule [55,56].

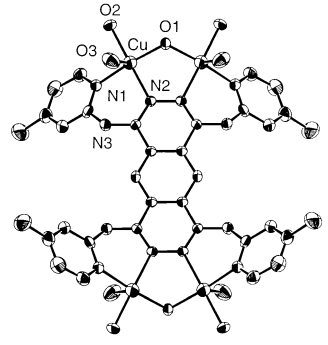

Fig. 9. Structural representation of $[Cu_4(diPAP4Me)(\mu\text{-}OH)_2(H_2O)_8](CF_3SO_3)_6$ (**9**).

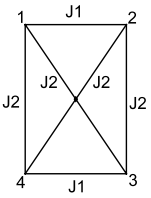

Scheme 6.

4.2. Self-assembled [2 × 2] grids

Polytopic ligands with contiguous coordination pockets arranged in a linear array can self assemble in the presence of a metal ion to form grid-like arrangements with metal ion spacings dependent on the size of the unit bridging the metal centers. Ligands like POAP (Scheme 7) have an alkoxide group which bridges two metal centers in close proximity, forming two contiguous five-membered chelate rings. Self assembly with M(II) salts (M = Mn, Co, Ni, Cu, Zn) produces [2 × 2] square tetranuclear grid structures in high yield (generally > 80%) [57,58]. Structures for the complexes $[Mn_4(POAPZ\text{–}H)_4(H_2O)_4]\ (NO_3)_4 \cdot H_2O$ (**10**), $[Ni_4(POAP\text{–}H)_4(H_2O)_4](NO_3)_4 \cdot 8H_2O$ (**11**), $[Co_4(PZOAPZ\text{–}H)_4(H_2O)_4]\ (ClO_4)_4 \cdot 3H_2O$ (**12**), and $[Zn_4(POAP\text{–}H)_4(H_2O)_4](NO_3)_5 \cdot 5.5H_2O$ (**13**), which are typical examples, are shown in Figs. 10–13, respectively. Four six-coordinate metal ions are bridged by four alkoxide oxygen atoms in a square [2 × 2] grid structure, with metal metal separations of ~4 Å and M–O–M angles in the range 133–141°. Two pairs of parallel ligands are arranged above and below the metal pseudo-planes with separations of 3.8–4.0 Å between the aromatic rings, indicating that the close proximity of the aromatic π-

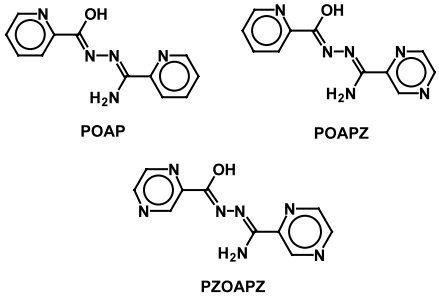

Scheme 7.

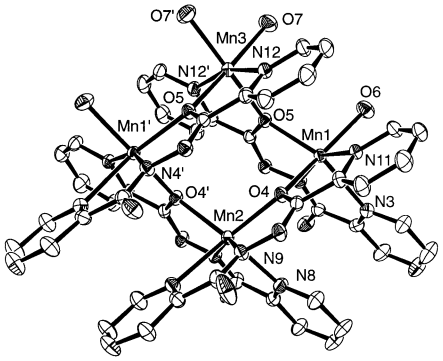

Fig. 10. Structural representation of $[Mn_4(POAPZ–H)_4(H_2O)_4](NO_3)_4 \cdot H_2O$ (**10**).

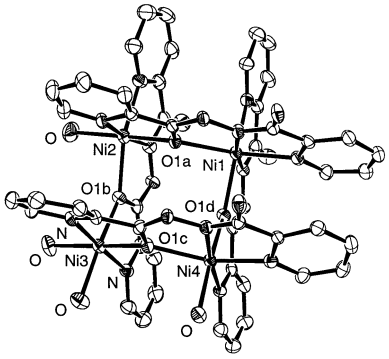

Fig. 11. Structural representation of $[Ni_4(POAP–H)_4(H_2O)_4](NO_3)_4 \cdot 8H_2O$ (**11**).

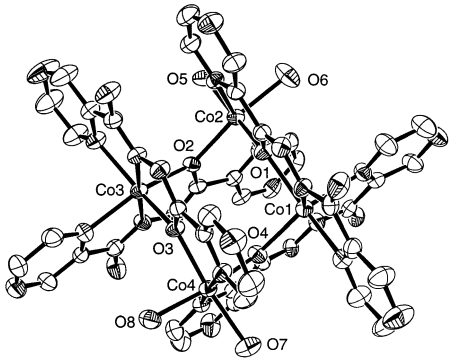

Fig. 12. Structural representation of $[Co_4(PZOAPZ–H)_4(H_2O)_4](ClO_4)_4 \cdot 3H_2O$ (**12**).

electron clouds is a significant factor in the arrangement of ligands and metal ions within the square (vide infra). Each ligand fills five coordination positions resulting in a non-homoleptic system, and so four additional ligands (water molecules for **10**–**13**) are required to complete the metal ion coordination spheres.

Copper forms similar complexes, but usually with a combination of five- and six-coordinate metal centers. $[Cu_4(POAPZ–H)_4(H_2O)](NO_3)_4 \cdot 3H_2O$ (**14**) is a typical example, and the core structure of the grid is shown in Fig. 14. A significant feature of the core bonding

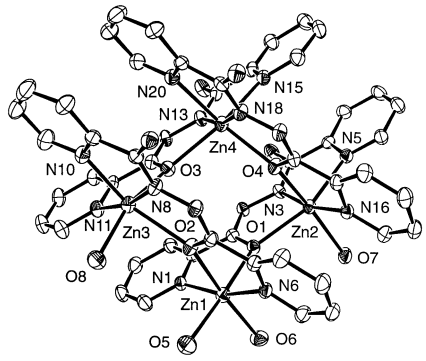

Fig. 13. Structural representation of $[Zn_4(POAP–H)_4(H_2O)_4](NO_3)_5 \cdot 5.5H_2O$ (**13**).

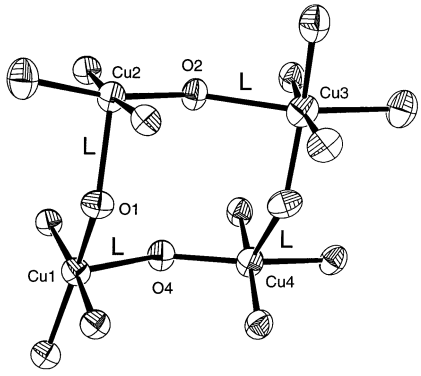

Fig. 14. Structural representation of the core in $[Cu_4(POAPZ–H)_4(H_2O)](NO_3)_4 \cdot 3H_2O$ (**14**).

connectivity is the axial-equatorial linkage between each adjacent pair of copper ions. The magnetic ground state of each copper is $d_{x^2-y^2}$, and so the alkoxide bridges link the metals orthogonally, leading to dominant ferromagnetic spin exchange (vide infra), despite large Cu–O–Cu bridge angles (139.8–141.0°).

Magnetic exchange within the square structure is dominated by antiferromagnetic coupling for the Mn(II), Co(II) and Ni(II) systems, as would be expected based on the large M–O–M bridge angles [57,58]. However, in the case of copper(II) the strict orthogonality between the metal magnetic orbitals imposed by the bridging connections leads to intramolecular ferromag-

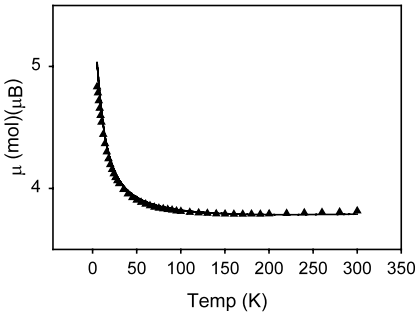

Fig. 15. Magnetic data for **14** (see text for fitted parameters).

netic coupling between the four copper(II) centers.

$$H_{ex} = -J(S_1 \cdot S_2 + S_2 \cdot S_3 + S_3 \cdot S_4 + S_1 \cdot S_4) \quad (4)$$

$$\chi_{M'} = \frac{N\beta^2 g^2}{3kT} \frac{\sum S_T(S_T+1)(2S_T+1)e^{-E(S_T)/kT}}{\sum S_T(2S_T+1)e^{-E(S_T)/kT}} \quad (5)$$

$$\chi_M = \chi_{M'}(1-\rho) + \frac{2N\beta^2 g^2 \rho}{3kT} + \mathrm{TIP} \quad (6)$$

The magnetic exchange model for square systems of this sort (e.g. Fig. 14) is defined by a Hamiltonian expression Eq. (4) involving just one exchange integral. The exchange expression can be derived by determining the total spin state combinations, and their energies, according to the Kambe coupling scheme [59], and substituting them into the van Vleck equation Eq. (5), but this is a tedious procedure. This can be done more conveniently using the MAGMUN-4.0 software package [60], which treats and solves the exchange situation for polynuclear complexes in a general way, without formally deriving an exchange equation.

The plot of μ(mol) versus temperature for **14** (Fig. 15) shows that moment rises as the temperature decreases, signifying intramolecular ferromagnetic exhange. A good fit of the data to Eqs. (4)–(6), for an isotropic square arrangement of four S = 1/2 centers gave $g = 2.119(7)$, $J = 9.8(4)$ cm^{-1}, $TIP = 234 \times 10^{-6}$ emu. mol^{-1} (solid line in Fig. 15). The ferromagnetic exchange was confirmed by a magnetization study as a function of field at 2 K, showing saturation at 5T, and an S = 2 ground state [57].

Ditopic ligands like POAP (Scheme 7), and its analogues, self assemble to produce tetranuclear square complexes with alkoxide bridges (vide supra). Separating the coordination pockets with an oxamide type bridge, e.g. in PAOH (Scheme 8), creates a ligand still capable of self assembly, and reaction with $Fe(ClO_4)_2$ and $CoBr_2$ produces tetranuclear square complexes $[Fe_4(PAOH)_4](ClO_4)_4$ (**15**) and $[Co_4(PAOH)_4]Br_8$ (**16**) [61]. The preliminary structure of **16** is shown in Fig. 16, and shows the square self assembled grid with the metal ions bonded at the ends of the ligands. **15** has a similar structure according to preliminary structural data [61].

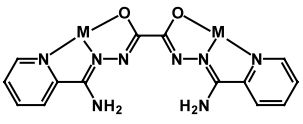

PAOH

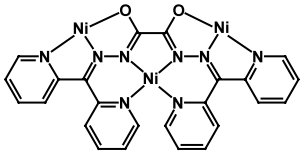

DPKOH

Scheme 8.

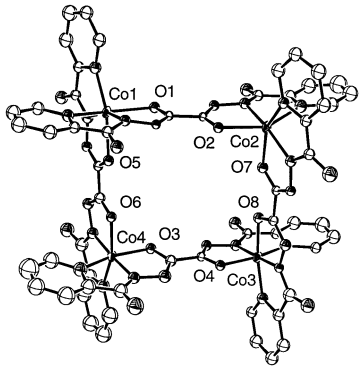

Fig. 16. Preliminary structural representation of $[Co_4(PAOH)_4]Br_8$ (**16**) (C2/c; $a = 32.6381(26)$ Å, $b = 17.8780(11)$ Å, $c = 35.9679(11)$ Å, $\beta = 116.952(2)$ Å; R1 = 0.149 (9399 data for $F_0 > 4.0F_0$).

Metal–metal distances fall in the range 6.78–7.25 Å (Fe) and 6.75–7.24 Å (Co). Unfortunately complete refinement of these structures has so far not been possible because of poor data sets and lattice disorder problems. However, the main cationic fragments are clearly defined. Variable temperature magnetic data for **15** indicate an essentially insignificant exchange interaction between the Fe(II) centers, clearly a function of the large distances of separation.

5. Pentanuclear complexes

The outcome of a self assembly process depends on a number of factors, including thermodynamic properties of the resulting products, and can lead to the formation of more than one oligomeric species. In the case of ligands like POAP (Scheme 7) the anion appears to have a significant influence on the oligomeric reaction outcome. The non-homoleptic tetranuclear complexes **10**–**13** have four open coordination sites, and almost exclusively form when the anion is nitrate, which in some cases is a ligand. With perchlorate the dominant products in the case of Mn(II), Co(II) and Zn(II) are homoleptic pentanuclear trigonal-bipyramidal clusters

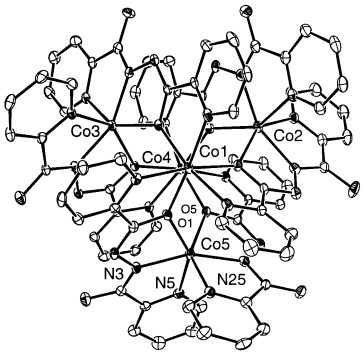

Fig. 17. Structural representation of $[Co_5(POAP–H)_6](ClO_4)_4 \cdot 3H_2O$ (**17**).

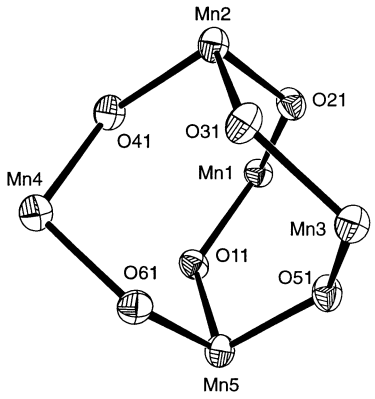

Fig. 18. Structural representation of the core in $[Mn_5(POAP–H)_6](ClO_4)_4 \cdot 3.5MeOH \cdot H_2O$ (**18**).

[62,63]. Fig. 17 shows the structure of $[Co_5(POAP–H)_6](ClO_4)_4 \cdot 3H_2O$ (**17**). Five Co(II) centers are arranged in a trigonal bipyramidal cluster with six alkoxide oxygen atoms from six ligands bridging the metal centers in a spiral-like fashion along the apical edges only. Each ligand fills five metal ion coordination sites resulting in an exact match between the coordination requirements of the five six-coordinate metals and the available donors (30). A similar structure was observed for $[Mn_5(POAP–H)_6](ClO_4)_4 \cdot 3.5MeOH \cdot H_2O$ (**18**) and $[Zn_5(POAP–H)_6](ClO_4)_4 \cdot 2.5H_2O$ (**19**), and a core structure for **18** showing the alkoxide bridging connections is depicted in Fig. 18. The M–O–M bridge angles fall in the range 128–137.2°.

The magnetic properties of **17** and **18** are dominated by intramolecular antiferromagnetic coupling with magnetic moment per mol dropping from 10.6 μ_B at 300 K to 2.7 μ_B at 2 K for **17**, and from 13.4 μ_B at 300 K to 6.0 μ_B at 2 K for **18**. Room temperature moments in each case are typical for five high spin metal centers. Fig. 19 shows the profile of χ_{mol} as a function of temperature for **18**. No attempt has been made to fit the data for **17** to a theoretical exchange expression, but for **18** the Hamiltonian

$$H_{ex} = -J(S_1 \cdot S_2 + S_2 \cdot S_3 + S_2 \cdot S_4 + S_5 \cdot S_4 + S_5 \cdot S_1 + S_5 \cdot S_3) \quad (7)$$

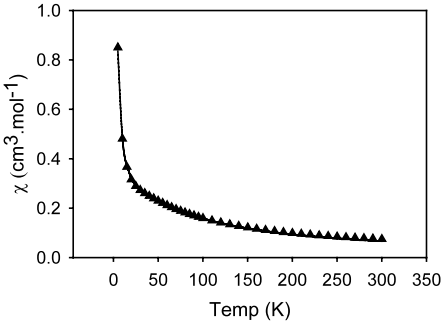

Fig. 19. Magnetic data for **18** (see text for fitting parameters).

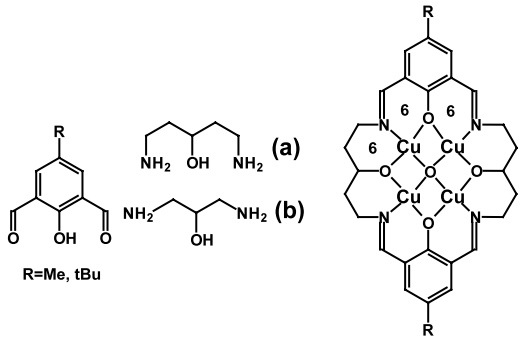

Scheme 9.

expression Eq. (7) describes a trigonal bi-pyramidal model based on Fig. 18, assuming a single exchange integral. Using the appropriate vector coupling scheme the spin states and their energies were calculated and substituted into the van Vleck equation Eq. (5) using MAGMUN [60], with corrections for TIP, Weiss-like temperature correction (θ) and paramagnetic impurity fraction (ρ) Eq. (6). The variable temperature data for **18** were fitted to modified Eq. (6) to give $g = 2.02(1)$, $J = -3.6(2)$ cm^{-1}, TIP $= 10 \times 10^{-6}$ cm^3 mol^{-1}, $\rho = 0.002$, $\theta = -0.5$ K. The solid line in Fig. 19 represents the fitting with the above parameters.

6. Hexanuclear template condensed macrocycles

2,6-Diformylphenols are difunctional dialdehydes, and condense with 1,5-diamino-3-hydroxypropane (Scheme 9—(a)) in the presence of transition metal salts, e.g. Cu(II) and Mn(II) to give tetranuclear macrocyclic derivatives, in which the metal centers are bridged by phenoxide and alkoxide oxygen atoms [64–67]. Other groups X (e.g. OH, O) can also act as exogenous central bridges. The chelate rings formed by this condensation process are all six-membered. Redu-

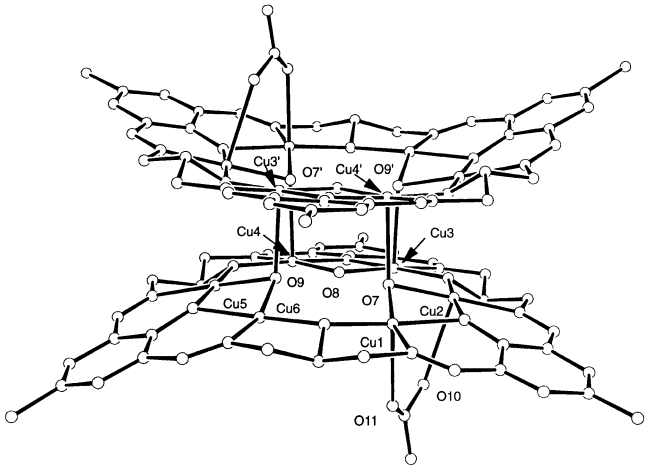

Fig. 20. Structural representation of $[(MME)Cu_6(\mu_2\text{-}OH)_3](NO_3)_3 \cdot 5H_2O$ (**19**).

cing the size of the diamino–alcohol to 1,3-diamino-2-hydroxypropane (b) leads to the formation of an alternating arrangement of pairs of adjacent five-membered and six-membered chelate rings, which becomes too strained to form an analogous tetranuclear structure, and allows the macocyclic ring to expand to include six metal ions in a 3+3 macrocyclic structural arrangement. Fig. 20 shows the structure of $[(MME)Cu_6(\mu_2\text{-}OH)_3](NO_3)_3.5H_2O$ (**19**) (MME, R = Me) [68,69]. The copper ions are bridged alternately with phenoxide and alkoxide oxygen atoms, with adventitious exogenous hydoxide groups bridging three copper pairs within the macrocyclic cavity. Cu–O(Phenoxide)–Cu angles fall in the range 96.1–97.8°, Cu–O(alkoxide)–Cu angles fall in the range 131.6–135.2°, and Cu–OH–Cu angles fall in the range 96.4–98.4°. The macrocyclic ring is distorted into a bowl-like shape, and two 'bowls' are linked at their bases by axial interactions via two hydroxides on each macrocycle to produce an associated dodecanuclear structure (Fig. 20).

The magnetic properties of **19** and the structurally similar complex $[(MTB)Cu_6(\mu_2\text{-}OH)_3](ClO_4)_3 \cdot 4H_2O$ (**20**) (MTB, R = *t*-Bu) are characterized by a maximum in χ_{mol} as a function of temperature at $T > 100$ K, and magnetic moments that drop steadily as temperature is lowered, indicating significant intra-molecular antiferromagnetic exchange. Fig. 21 shows the plot of μ_{mol} versus temperature for **20.** The data have been fitted to an exchange expression derived from the Hamiltonian Eq. (8), which assumes for simplicity that within the hexanuclear ring exchange terms are effectively the same, despite the difference in the bridging groups.

$$H_{ex} = -J(S_1 \cdot S_2 + S_2 \cdot S_3 + S_3 \cdot S_4 + S_4 \cdot S_5 + S_5 \cdot S_6 + S_1 \cdot S_6) \quad (8)$$

The solid line in Fig. 21 is calculated for $g = 2.04$, $J = -260$ cm^{-1}, TIP $= 440 \times 10^{-6}$ cm^3 mol^{-1}, $\rho = 0.003$, $\theta = -5$ K, $10^2R = 4.7$ ($R = [\Sigma(\chi_{obs} - \chi_{calc})^2/\Sigma\chi^2_{obs}]^{1/2}$). A similar fit for 19 gave $g = 2.05$, $J = -159.2$ cm^{-1}, $\rho = 0.019$. A preliminary structural analysis of 20 showed that Cu–O–Cu angles throughout the structure are significantly larger than those in 19, in agreement with the stronger antiferromagnetic exchange within the Cu_6 ring. The difference in *J* values reported here, and those reported previously rests with an apparent error in reference [69], which reports *J* as twice the correct value. While the magnetic properties of these systems can be modeled with two alternating and different *J* values around the Cu_6 ring, associated with the different bridging groups, the model is not considered to be an improvement, and the most reasonable result is that assuming a single exchange integral, and an effective equivalent involvement of all six copper atoms in the exchange process.

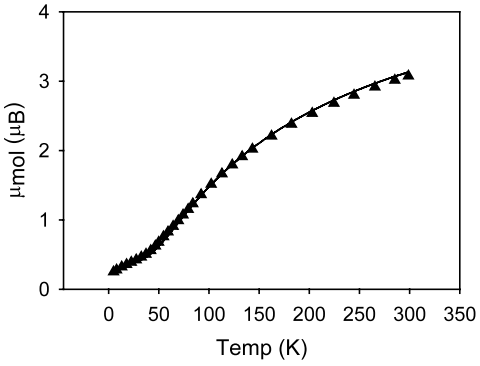

Fig. 21. Magnetic data for $[(MTB)Cu_6(\mu_2\text{-}OH)_3](ClO_4)_3 \cdot 4H_2O$ (**20**) (see text for fitting parameters).

7. Octanuclear rings and clusters

A slight modification of the ligand PAOH to produce the 'tritopic' tetrapyridyl ligand DPKOH (Scheme 8) can potentially lead to a self assembled grid based on a [2 × 2] square arrangement similar to **15** and **16**, but with an extra metal ion bound on the edge of the square. Reaction of DPKOH with $Ni(BF_4)_2 \cdot 6H_2O$ in methanol/water produced a red–brown crystalline solid $[Ni_8(DPKOH\text{–}2H)_4(H_2O)_8](BF_4)_8 \cdot 16H_2O$ (**21**) in high yield [70]. The structure of the octanuclear cation is shown in Fig. 22, revealing a square grouping of six-coordinate Ni(II) centers (Ni(1), Ni(3), Ni(5), Ni(7)), with a roughly tetrahedral grouping of six-coordinate Ni(II) centers (Ni(2), Ni(4), Ni(6), Ni(8)) arranged in the external ligand pockets. The external Ni(II) centers are bound to two axial water molecules. The core structure is shown in Fig. 23, which reveals that the important bridging connections between adjacent metal ions in the ring are μ_2-N_2 diazine groups with an almost *trans* arrangement (Ni–N–N–Ni 154–173°). Variable temperature magnetic data show a sharp drop in magnetic moment from 8.3 μ_B at 300 K to 2.7 μ_B at 2 K. Fitting of

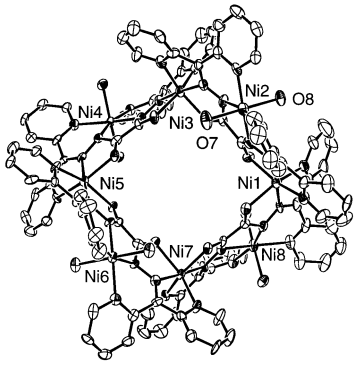

Fig. 22. Preliminary structural representation for solid $[Ni_8(DPKOH\text{–}2H)_4(H_2O)_8](BF_4)_8 \cdot 16H_2O$ (**21**) ($P2_1/n$; $a = 21.153(5)$ Å, $b = 35.778(9)$ Å, $c = 21.823(5)$ Å, $\beta = 97.757(6)$ Å, $R1 = 0.140$, $wR2 = 0.446$ for 10479 unique reflections with $I > 2.0\sigma(I)$ (33447 independent reflections, $R_{int} = 0.241$).

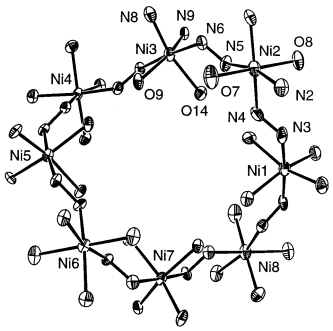

Fig. 23. Structural representation of the core in **21**.

the magnetic data to an isotropic exchange expression based on the Hamiltonian expression Eq. (9) using MAGMUN [59,60] gave a good fit with $g = 2.250(5)$, $J = -15.0(4)$ cm^{-1}, TIP = 0.00150 cm^3 mol^{-1}. The strong antiferromagentic coupling is

$$H_{ex} = -J[S_i \cdot S_{i+1} + S_8 \cdot S_1](i = 1-7) \quad (9)$$

consistent with other complexes having close to *trans* N–N bridging interactions [41–43].

The 'tritopic' ligand 2POAP (Scheme 5) forms trinuclear complexes in a few cases (vide supra), where strongly donating anions and solvent are involved (**7**, **8**). However, in most cases strict self assembly occurs with MX_2 (M = Mn(II), Co(II), Ni(II), Cu(II), Zn(II); X = NO_3, ClO_4) (vide infra) to form homoleptic [3 × 3] nine metal square grids. In one unique case reaction of 2POAP with $Gd(NO_3)_2$ followed by $Cu(NO_3)_2$ produced an unusual octanuclear $Cu(II)_8$ cluster (Fig. 24) in the complex $[Cu_8(2POAP)_4CH_3OH)_4(CH_3CN)_4][Gd(NO_3)_4(H_2O)_2]_2(NO_3)_6 1.3Cu(NO_3)_2 \cdot 10H_2O$ (**22**), with four ligands arranged with their ends assembled in a square $Cu_4(\mu\text{-}O)_4$ grid arrangement similar to the [2 × 2] grids formed by POAP and related ligands (Scheme 7) (the Gd and extra Cu(II) centers are located in the lattice, and are not connected to the octanuclear cluster). The external ligand pockets bind four extra Cu(II) ions forming a 'pin-wheel' like cluster with the external copper centers bridged to the square core with alkoxide

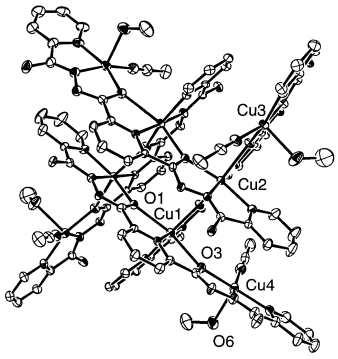

Fig. 24. Structural representation of the octanuclear cation in $([Cu_8(2POAP)_4(CH_3OH)_4\ (CH_3CN)_4][Gd(NO_3)_4(H_2O)_2]_2(NO_3)_6 1.3Cu(NO_3)_2 \cdot 10H_2O$ (**22**).

bridges. Other coordination sites are occupied by solvent molecules (methanol, acetonitrile). All the bridging connections between adjacent Cu(II) centers are orthogonal (axial/equatorial), and so despite quite large Cu–O–Cu angles (139–142°) antiferromagetic coupling would not be expected to be significant. The observed ferromagnetic coupling in this system ($g_{ave.} = 2.113(2)$, $J = 5.0(2)$ cm^{-1}, TIP = 500 × 10^{-6} cm^3 mol^{-1}; exchange expression based on an exchange Hamiltonian Eq. (10) assuming a pin-wheel

$$H_{ex} = -J(S_1 \cdot S_2 + S_2 \cdot S_3 + S_3 \cdot S_4 + S_1 \cdot S_4 + S_1 \cdot S_5 + S_2 \cdot S_6 + S_3 \cdot S_7 + S_4 \cdot S_8) \quad (10)$$

cluster with a single J value; MAGMUN [59,60]) is consistent with the structure and other similar Cu(II) grids [71].

8. Nonanuclear [3 × 3] grids

2POAP and related ligands (Scheme 5) self assemble in high yield (usually > 80%) with Fe(III), Mn(II), Co(II), Ni(II), Cu(II) and Zn(II) salts (e.g. nitrate, perchlorate) to give homoleptic, square [3 × 3] nonanuclear grid structures with six heptadentate ligands enclosing the nine metals. A typical structure of $[Mn_9(2POAP–2H)_6](ClO_4)_6 \cdot 3.75CH_3CN \cdot 11H_2O$ (**23**) is shown in Fig. 25, which shows the six ligands arranged in two parallel sets of three arranged above and below the $Mn_9(\mu_2\text{-}O)_{12}$ core arrangement of the six-coordinate Mn(II) centers [53]. The core itself is shown in Fig. 26. Mn–Mn distances fall in the range 3.88–4.03 Å and Mn–O–Mn angles in the range 126.6–130.0°. The large alkoxide bridge angles would suggest that the magnetic properties of this grid would be dominated by intramolecular antiferromagnetic exchange, and this is confirmed with variable temperature studies showing a

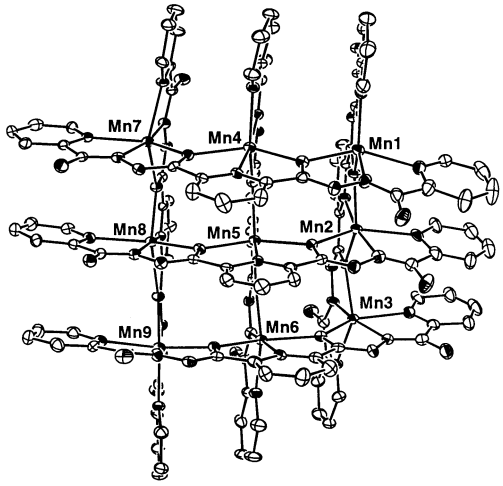

Fig. 25. Structural representation of the nona-nuclear cation in $[Mn_9(2POAP–2H)_6]\ (ClO_4)_6 \cdot 3.75CH_3CN \cdot 11H_2O$ (**23**).

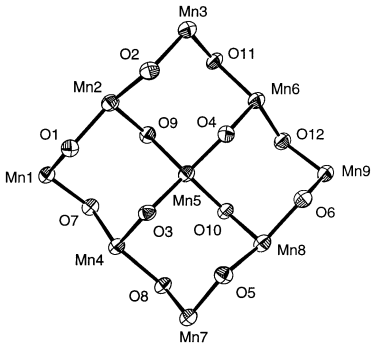

Fig. 26. Structural representation of the $Mn_9(\mu\text{-}O)_{12}$ core in **23**.

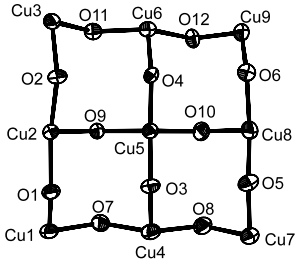

Fig. 27. Structural representation of the $Cu_9(\mu\text{-}O)_{12}$ core in $[Cu_9(2POAP{-}H)_6](NO_3)_{12}\cdot 9H_2O$ (**24**).

marked drop in magnetic moment from 16.9 μ_B (mol) at 300 K to 6.9 μ_B at 5 K. One remarkable feature of this and related Mn_9 systems is a rich electrochemistry, which shows an eight electron redox process in the range 0.5–1.6 V (vs. SCE) in acetronitrile, associated with sequential oxidation of eight Mn(II) centers to Mn(III) [53].

A related Cu_9 complex, $[Cu_9(2POAP{-}H)_6](NO_3)_{12}\cdot 9H_2O$ (**24**) has a similar $[3\times 3]$ grid structure with comparable metal separations, but Cu–O–Cu bridge angles which are substantially larger (136.5–143.6°). The core structure of **24** is shown in Fig. 27. The nine pseudo-octahedral copper centers are bridged in a unique arrangement with axial/equatorial connections between all metal ions. The central copper (Cu5) has a compressed tetragonal d_{z^2} ground state, with long Cu–O equatorial connections. The variable temperature magnetic properties reveal a mixture of antiferromagnetic and ferromagnetic exchange coupling. The magnetic moment per mol varies as a function of temperature (Fig. 28) with a drop from 6.4 μ_B at 300 K to 5.5 μ_B at 25 K, followed by a sharp rise to 6.9 μ_B at 2 K. The data were fitted to an isotropic exchange equation within MAGMUN [59,60], which is based on a Hamiltonian Eq. (11), which assumes two significant exchange pathways; JR in the external Cu_8 ring, and JC from the central copper Cu5 to its immediate neighbors.

$$H_{ex} = -\mathrm{JR}(S_1\cdot S_2 + S_2\cdot S_3 + S_3\cdot S_6 + S_6\cdot S_9 + S_8\cdot S_9 + S_7\cdot S_8 + S_4\cdot S_7 + S_1\cdot S_4) - \mathrm{JC}(S_2\cdot S_5 + S_6\cdot S_5 + S_8\cdot S_5 + S_4\cdot S_5) \quad (11)$$

The data were fitted to this expression using MAGMUN [59,60] to give $g = 2.30$, $\mathrm{JR} = 0.52\ \mathrm{cm}^{-1}$, $\mathrm{JC} = -24.3\ \mathrm{cm}^{-1}$, $\mathrm{TIP} = 200\times 10^{-6}$ emu (solid line in Fig. 28) [72–74]). Despite the fact that Cu5 appears to have a d_{z2} ground state according to the structure, it is antiferromagnetically coupled ($\mathrm{JC} = -24.3\ \mathrm{cm}^{-1}$) to its immediate neighbors, and so must undergo a dynamic Jahn–Teller distortion effect, where in its relationship with one equivalent neighboring copper center it appears to be $d_{x^2-y^2}$. JR (ferromagnetic) clearly dominates at low temperature and, therefore, leads to an effective S = 7/2 low temperature ground state, in agreement with magnetization versus field data at 2 K. A detailed study of the magnetic anisotropy of this system has been reported [74].

A comparison of the Cu_9 grid with related Cu_4 $[2\times 2]$ grids (e.g. **14**) shows that the ferromagnetic exchange term (JR) differs considerably for what are comparable bonding connections, and is much weaker. While it is inherently more difficult to quantify ferromagnetic exchange situations than antiferromagnetic cases, the much stronger antiferromagnetic JC term in **24** must have a direct influence on the magnitude of the ring (JR) exchange situation, and appears to diminish it.

A $[3\times 3]$ $Ag(I)_9$ grid has been reported with a pyridazine bridging ligand [75], but as far as we are aware, complexes like **23** and **24** are the first reported examples of magnetic grids in this class.

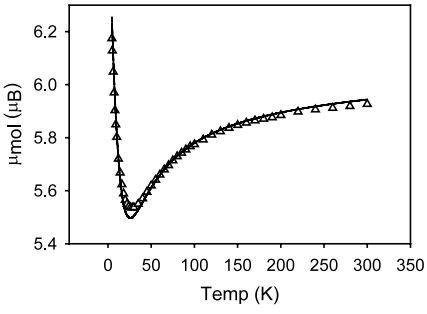

Fig. 28. Magnetic data for **24** (see text for fitted parameters).

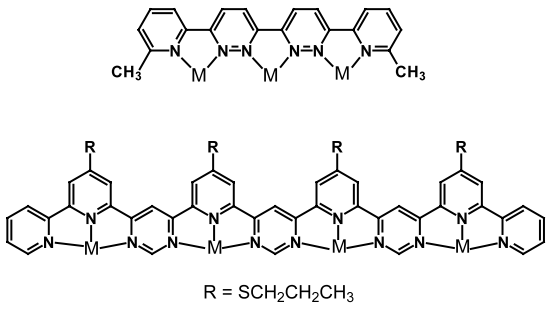

Scheme 10.

9. Predictable higher order polynuclear assemblies

While high nuclearity clusters can be produced by self assembly reactions of transition metal salts with simple ambidentate bridging ligands, e.g. 2-hydroxypyridines, the control that can be exerted over the oligomeric outcome is rather limited [see for example [76] [77] [78] [79]]. Linear polytopic ligands, with well defined coordination pocket arrangements, self assemble in high yields in most cases to produce predictable high nuclearity grids, with examples of [3 × 3] and [4 × 4] square structures. Ligands like 2POAP (Scheme 5) produce [3 × 3] magnetic grids on self assembly with transition metal ions with weakly coordinating anions, and pyridazine and pyrimidine based ligands (Scheme 10) have been shown to produce a non-magnetic [3 × 3] $[Ag(I)_9L_6]$ grid [74] and a putative square [4 × 4] $[Pb(II)_{16}L_8]$ grid [80], respectively. The ligands generate five-membered chelate rings on coordination, but the pyridazine ligand can only accommodate a four-coordinate metal ion, while the pyrimidine ligand can accommodate six-ccordinate metal ions.

The generation of ligands capable of extending the size of the grids will be tempered by the complexity of the organic synthetic routes required to produce them. However, several features are considered to be critical. The coordination pockets must involve five-membered chelate rings, and the pockets must be arranged in a contiguous linear grouping. For systems with significant anticipated magnetic interactions within the grid the pockets should be separated by short bridging connections, particularly single atom bridges, e.g. alkoxide as in 2POAP and related ligands, so that magnetic orbital overlap between adjacent metal ions is significant. The presence of aromatic rings is also seen as a significant contributing factor to the stability of the resulting grid because the parallel alignment of the ligands is enhanced as the π electron clouds come into close proximity. As part of our ongoing studies to achieve this goal we are attempting to extend the precursor hydrazide subunits used to produce ligands like 2POAP with extra compartments, while maintaining the alternating sequence of O and N donors. It is not unreasonable to expect examples of larger (e.g. [4 × 4] and higher) magnetic grids in the future.

10. High nuclearity clusters and grids—potential utility

The synthetic organization of paramagnetic metal centers into closely spaced arrays such that magnetic communication leads to cooperative bulk magnetic properties is a special challenge, and is generally achieved by having small bridging groups, which produce extended 2D and 3D structural arrangements. Cyanide has proven to be useful in this regard, and with orthogonally connected metal orbitals long range ferromagnetic ordering can be achieved in the interlocking cubic structured Prussian blue type systems, e.g. $CsNi(II)[Cr(III)(CN)_6] \cdot 2H_2O$ ($T_c = 90$ K) [81]. If interacting orbitals are not orthogonal the resulting antiferromagnetic exchange in this type of structure can lead to overall ferrimagnetic coupling and comparable T_c values (e.g. 90 K in $CsMn(II)[Cr(III)(CN)_6] \cdot H_2O$) [82]. Much higher T_c values have been obtained with non-stoichiometric complexes, e.g. $V(II/III)[Cr(III)(CN)_6]_{0.86} \cdot 2.8H_2O$ (ferrimagnet ordering > 315 K) [83], and $KV(II)[Cr(III)(CN)_6] \cdot 2H_2O$ (ferrimagnet ordering at 376 K) [84].

The optimal organizing of paramagnetic transition metal centers into extended bridged structures with very short metal ion spacings can only be achieved with single atom bridges. This cannot be done with, e.g. cyanide bridges, but can be approached with, e.g. oxygen based bridges. We have set the stage in the area of small 2D arrays with many examples of [3 × 3] magnetic grids with Mn(II), Co(II), Ni(II) and Cu(II) salts, where M–M separations are of the order of 4 Å. Thus far with the exception of Cu(II) all the systems studied exhibit intramolecular antiferromagnetic exchange, due to non-orthogonal bridging connections. The unexpected ferromagnetic character of the $Cu(II)_9$ systems augers well for novel properties in larger grids, and the highly unusual electrochemistry of the $Mn(II)_9$ grids suggests that Mn(II)/Mn(III) systems can be isolated, which may exhibit novel magnetic properties, and form the basis for individual molecule perturbation and information storage. A [2 × 2] self assembled $Fe(II)_4$ grid reported by Lehn, based on a pyrimidine bridging framework shows novel spin crossover behavior induced by temperature, pressure and light perturbations [85]. These important single molecule attributes can only be exploited if individual molecules can be successfully addressed. Surface deposition has been achieved with a related square [2 × 2] cationic $Co(II)_4$ grid monolayer arrangement on a pyrolytic graphite surface, with individual cations being addressed using STM probe techniques [86]. Efforts to examine this behavior with our [3 × 3] magnetic grids and larger analogues will be undertaken, and in particular methods explored for the electrochemical probing of surface deposited high nuclearity Mn(II) grids.

Acknowledgements

The unfailing support of numerous graduate and undergraduate students, Postdoctoral Fellows and Research Associates, who contributed to this work, and financial support from NSERC (Natural Sciences and Engineering Research Council of Canada), and Memorial University are gratefully acknowledged.

References

[1] S.J. Lippard, J.L. Berg, Principles of Bioinorganic Chemistry (University Science Books), Mill Valley, CA, 1994.
[2] A. Messerchmidt, A. Rossi, R. Ladenstein, R. Huber, M. Bolognesi, G. Gatti, A. Marchesini, R. Petruzzelli, A. Finazzi-Agró, J. Mol. Biol. 206 (1989) 513.
[3] L.K. Thompson, V.T. Chacko, J.A. Elvidge, A.B.P. Lever, R.V. Parish, Can. J. Chem. 47 (1969) 4141.
[4] M. Ghedini, G. De Munno, G. Denti, A.M. Manotti Lanfredi, A. Tiripicchio, Inorg. Chim. Acta 57 (1982) 87.
[5] P. Dapporto, G. De Munno, G. Bruno, M. Romeo, Acta Crystallogr. C39 (1983) 718.
[6] P. Dapporto, G. De Munno, A. Sega, L. Mealli, Inorg. Chim. Acta 83 (1984) 171.
[7] G. De Munno, G. Denti, Acta Crystallogr. C40 (1984) 616.
[8] G. De Munno, G. Denti, P. Dapporto, Inorg. Chim. Acta 74 (1983) 199.
[9] G. De Munno, G. Bruno, Acta Crystallogr. C40 (1984) 2022.
[10] D. Attanasio, V. Fares, P. Imperatori, J. Chem. Soc. Chem. Commun. (1986) 1476.
[11] A. Tiripicchio, A. M. Manoti Lanfredi, M. Ghedini, F. Neve, J. Chem. Soc. Chem. Commun. (1983) 97.
[12] J.E. Andrew, A.B. Blake, J. Chem. Soc. A (1969) 1408.
[13] P.W. Ball, A.B. Blake, J. Chem. Soc. A (1969) 1415.
[14] P.W. Ball, A.B. Blake, J. Chem. Soc. Dalton Trans. (1974) 852.
[15] A.B.P. Lever, L.K. Thompson, W.M. Reiff, Inorg. Chem. 11 (1972) 104.
[16] L.K. Thompson, Can. J. Chem. 61 (1983) 579.
[17] L.K. Thompson, A.W. Hanson, B.S. Ramaswamy, Inorg. Chem. 23 (1984) 2459.
[18] L.K. Thompson, F.W. Hartstock, P. Robichaud, A.W. Hanson, Can. J. Chem. 62 (1984) 2755.
[19] S.K. Mandal, L.K. Thompson, A.W. Hanson, J. Chem. Soc. Chem. Commun. (1985) 1709.
[20] L.K. Thompson, T.C. Woon, D.B. Murphy, E.J. Gabe, F.L. Lee, Y. LePage, Inorg. Chem. 24 (1985) 4719.
[21] L.K. Thompson, S.K. Mandal, E.J. Gabe, J-P. Charland, J. Chem. Soc. Chem. Commun. (1986) 1537.
[22] L. Rosenberg, L.K. Thompson, E.J. Gabe, F.L. Lee, J. Chem. Soc. Dalton Trans. (1986) 625.
[23] S.K. Mandal, L.K. Thompson, M.J. Newlands, F.L. Lee, Y. LePage, J-P. Charland, E.J. Gabe, Inorg. Chim. Acta 122 (1986) 199.
[24] S.K. Mandal, T.C. Woon, L.K. Thompson, M.J. Newlands, E.J. Gabe, Aust. J. Chem. 39 (1986) 1007.
[25] L.K. Thompson, S.K. Mandal, E.J. Gabe, F.L. Lee, A.W. Addison, Inorg. Chem. 26 (1987) 657.
[26] L.K. Thompson, S.K. Mandal, L. Rosenberg, F.L. Lee, E.J. Gabe, Inorg. Chim. Acta 133 (1987) 81.
[27] L.K. Thompson, F.L. Lee, E.J. Gabe, Inorg. Chem. 27 (1988) 39.
[28] L.K. Thompson, S.K. Mandal, J-P. Charland, E.J. Gabe, Can. J. Chem. 66 (1988) 348.
[29] T. Wen, L.K. Thompson, F.L. Lee, E.J. Gabe, Inorg. Chem. 27 (1988) 4190.
[30] S.K. Mandal, L.K. Thompson, M.J. Newlands, J-P. Charland, E.J. Gabe, Inorg. Chim. Acta 178 (1990) 169.
[31] S.S. Tandon, L.K. Thompson, R.C. Hynes, Inorg. Chem. 31 (1992) 2210.
[32] L. Chen, L.K. Thompson, J.N. Bridson, Inorg. Chem. 32 (1993) 2938.
[33] L. Chen, L.K. Thompson, J.N. Bridson, Inorg. Chim. Acta 214 (1993) 67.
[34] S.S. Tandon, L. Chen, L.K. Thompson, J.N. Bridson, Inorg. Chem. 33 (1994) 490.
[35] S.S. Tandon, L.K. Thompson, J.N. Bridson, J.Chem. Soc. Chem. Commun. (1993) 804.
[36] S.S. Tandon, L.K. Thompson, M.E. Manuel, J.N. Bridson, Inorg. Chem. 33 (1994) 5555.
[37] L.K. Thompson, S.S. Tandon, M.E. Manuel, Inorg. Chem. 34 (1995) 2356.
[38] S.S. Tandon, L.K. Thompson, D.O. Miller, J. Chem. Soc. Chem. Commun. (1995) 1907.
[39] L.K. Thompson, S.S. Tandon, Comments Inorg. Chem. 18 (1996) 125.
[40] C.L. Sheppard, S.S. Tandon, L.K. Thompson, J.N. Bridson, D.O. Miller, M. Handa, F. Lloret, Inorg. Chim. Acta 250 (1996) 227.
[41] Z. Xu, L.K. Thompson, D.O. Miller, Inorg. Chem. 36 (1997) 3985.
[42] L.K. Thompson, Z. Xu, A.E. Goeta, J.A.K. Howard, H.J. Clase, D.O. Miller, Inorg. Chem. 37 (1998) 3217.
[43] Z. Xu, L.K. Thompson, D.O. Miller, H.J. Clase, J.A.K. Howard, A.E. Goeta, Inorg. Chem. 37 (1998) 3620.
[44] Z. Xu, L.K. Thompson, C.J. Matthews, D.O. Miller, A.E. Goeta, C. Wilson, J.A.K. Howard, M. Ohba, H. Ōkawa, J. Chem. Soc. Dalton Trans. (2000) 69.
[45] Z. Xu, S. White, L.K. Thompson, D.O. Miller, M. Ohba, H. Ōkawa, C. Wilson, J.A.K. Howard, J. Chem. Soc. Dalton Trans. (2000) 1751.
[46] Z. Xu, L.K. Thompson, D.A. Black, C. Ralph, D.O. Miller, M.A. Leech, J.A.K. Howard, J. Chem. Soc. Dalton Trans. (2001) 2042.
[47] V.H. Crawford, H.W. Richardson, J.R. Wasson, D.J. Hodgson, W.E. Hatfield, Inorg. Chem. 15 (1976) 2107.
[48] O. Kahn, Inorg. Chim. Acta 62 (1984) 3.
[49] S. Sikorav, I. Bkouche-Waksman, O. Kahn, Inorg. Chem. 23 (1984) 490.
[50] M-F. Charlot, O. Kahn, M. Chaillet, C. Larrieu, J. Am. Chem. Soc. 108 (1986) 2574.
[51] M.A Aebersold, B. Gillon, O. Plantevin, L. Pardi, O. Kahn, P. Bergerat, I. Von Seggern, F. Tuczek, L. Öhrström, A. Grand, E. Lelièvre-Berna, J. Am. Chem. Soc. 120 (1998) 5238.
[52] E. Ruiz, J. Cano, S. Alvarez, P. Alemany, J. Am. Chem. Soc. 120 (1998) 11122.
[53] L. Zhao, C.J. Matthews, L.K. Thompson, S.L. Heath, J. Chem. Soc. Chem. Commun. (2000) 265.
[54] L. Zhao, L.K. Thompson, Z. Xu, D.O. Miller, D.R. Stirling, J. Chem. Soc. Dalton Trans. (2001) 1706.
[55] S.S. Tandon, S.K. Mandal, L.K. Thompson, R.C. Hynes, J. Chem. Soc. Chem. Commun. (1991) 572.
[56] S.S. Tandon, S.K. Mandal, L.K. Thompson, R.C. Hynes, Inorg. Chem. 31 (1992) 2215.
[57] C.J. Matthews, K. Avery, Z. Xu, L.K. Thompson, L. Zhao, D.O. Miller, K. Biradha, K. Poirier, M.J. Zaworotko, C. Wilson, A.E. Goeta, J.A.K. Howard, Inorg. Chem. 38 (1999) 5266.
[58] L.K. Thompson, C.J. Matthews, L. Zhao, Z. Xu, D.O. Miller, C. Wilson, M.A. Leech, J.A.K. Howard, S.L. Heath, A.G. Whittaker, R.E.P. Winpenny, J. Solid State Chem. 159 (2001) 308.
[59] K. Kambe, J. Phys. Soc. Jpn. 5 (1950) 38.
[60] MAGMUN-4.0 is available free of charge. It has been developed by Dr. Zhiqiang Xu (Memorial University, http://www.chem.-mun.ca/resinst/) and Kathy He in collaboration with Prof. L.K. Thompson (lthomp@mun.ca), and Dr. O. Waldmann (waldmann@physik.uni-erlangen.de). We do not distribute the source codes. The programs may be used only for scientific purposes, and economic utilization is not allowed. If either routine is used to obtain scientific results, which are published, the origin of the programs should be quoted.
[61] L. Zhao, L.K. Thompson J.A.K. Howard, Unpublished results.
[62] C.J. Matthews, Z. Xu, S.K. Mandal, L.K. Thompson, K. Biradha, K. Poirier, M.J. Zaworotko, J. Chem. Soc. Chem. Commun. (1999) 347.

[63] C.J. Matthews, L.K. Thompson, S.R. Parsons, Z. Xu, D.O. Miller, S.L. Heath, Inorg. Chem. 40 (2001) 4448.
[64] V. McKee, S.S. Tandon, J. Chem. Soc. Chem. Commun. (1988) 385.
[65] V. McKee, S.S. Tandon, J. Chem. Soc. Chem. Commun. (1988) 1334.
[66] V. McKee, S.S. Tandon, Inorg. Chem. 28 (1989) 2902.
[67] V. McKee, S.S. Tandon, J. Chem. Soc. Dalton Trans. (1991) 221.
[68] S.S Tandon, L.K. Thompson, J.N. Bridson, J. Chem. Soc. Chem. Commun. (1992) 911.
[69] S.S. Tandon, L.K. Thompson, J.N. Bridson, C. Benelli, Inorg. Chem. 34 (1995) 5507.
[70] V.A. Milway, L.K. Thompson D.O. Miller, Unpublished results.
[71] Z. Xu, L.K. Thompson, D.O. Miller, J. Chem. Soc. Chem. Commun. (2001) 1170.
[72] L. Zhao, Z. Xu, L.K. Thompson, S.L. Heath, D.O. Miller, M. Ohba, Angew. Chem. Int. Ed. 39 (2000) 3114.
[73] L. Zhao, Z. Xu, L.K. Thompson, D.O. Miller, Polyhedron 20 (2001) 1369.
[74] O. Waldmann, R. Koch, S. Schromm, P. Müller, L. Zhao, L.K. Thompson, Chem. Phys. Lett. 332 (2000) 73.
[75] P.N.W. Baxter, J-M. Lehn, J. Fischer, M-T. Youinou, Angew. Chem. Int. Ed. 33 (1994) 2284.
[76] A.J. Blake, C.M. Grant, S. Parson, J.M. Rawson, R.E.P. Winpenny, J. Chem. Soc. Chem. Commun. (1994) 2363.
[77] E.K. Brechin, S. Parsons, R.E.P Winpenny, J. Chem. Soc. Dalton Trans. (1996) 3745.
[78] E.K. Brechin, A. Graham, S.G. Harris, S. Parsons, R.E.P. Winpenny, J. Chem. Soc. Dalton Trans. (1997) 3405.
[79] E.K. Brechin, S.G. Harris, A. Harrison, S. Parsons, A.G. Whittaker, R.E.P. Winpenny, Chem. Commun. (1997) 653.
[80] A.M. Garcia, F.J. Romero-Salguero, D.M. Bassani, J-M. Lehn, G. Baum, D. Fenske, Chem. Eur. J. 5 (1999) 1803.
[81] V. Gadet, T. Mallah, I. Castro, M. Verdaguer, P. Veillet, J. Am. Chem. Soc. 114 (1992) 9213.
[82] W.R Entley, C.R. Treadway, G.S. Girolami, Mol. Crystallogr. Liq. Crys. 273 (1995) 153.
[83] S. Ferlay, T. Mallah, R. Ouahes, P. Veillet, M. Verdaguer, Nature 387 (1995) 701.
[84] S.D. Holmes, G. Girolami, J. Am. Chem. Soc. 121 (1999) 5593.
[85] E. Breuning, M. Ruben, J-M. Lehn, F. Renz, Y. Garcia, V. Ksenofontov, P. Gütlich, E. Wegelius, K. Risannen, Angew. Chem. Int. Ed. 39 (2000) 2504.
[86] A. Semenov, J.P. Spatz, M. Möller, J.-M. Lehn, B. Sell, D. Schubert, C.H. Weidl, U.S. Schubert, Angew. Chem. Int. Ed. 38 (1999) 2547.